Available online at www.sciencedirect.com
SCIENCE DIRECT®
Journal of Solid State Chemistry 177 (2004) 119–125
JOURNAL OF SOLID STATE CHEMISTRY
http://elsevier.com/locate/jssc

Magnetism and structural chemistry of the $n=2$ Ruddlesden–Popper phase La_3LiMnO_7

Peter D. Battle,[a,*] Jonathan C. Burley,[b] Daniel J. Gallon,[a] Clare P. Grey,[c] and Jeremy Sloan[a]

[a] *Inorganic Chemistry Laboratory, Oxford University, South Parks Road, Oxford OX1 3QR, UK*
[b] *Materials Science Division, Argonne National Laboratory, Argonne, IL 60439, USA*
[c] *Chemistry Department, State University of New York at Stony Brook, Stony Brook, NY 11794-3400, USA*

Received 8 January 2003; received in revised form 30 May 2003; accepted 5 June 2003

Abstract

Polycrystalline samples of the $n=2$ Ruddlesden–Popper phase La_3LiMnO_7 have been prepared and characterized. X-ray and neutron diffraction suggest that the structure is tetragonal with a disordered distribution of Li and Mn cations over the octahedral sites, but ^{6}Li MAS NMR shows that the Li and Mn are 1:1 ordered locally. Electron microscopy shows that the stacking of the cation-ordered, perovskite-like bilayers along the crystallographic z-axis is disordered on the distance scale sampled by X-ray and neutron diffraction. Magnetometry data and neutron diffraction data collected at 2 K together suggest that the Mn cations within each structural domain order antiferromagnetically at 14 K, but that the disorder along z prevents the establishment of long-range magnetic order.

Keywords: Ruddlesden–Popper; Cation order; Stacking fault

1. Introduction

Recent research into the phenomenon of colossal magnetoresistance (CMR) has increased interest in the structural and magnetic properties of those mixed-metal oxides of manganese which can be formulated as $(A_{1-y}A'_y)_{n+1}Mn_nO_{3n+1}$, where A and A' are usually lanthanide or alkaline earth cations. The structures of these compounds, known as Ruddlesden–Popper phases [1], consist of blocks built up from perovskite-like sheets of vertex-sharing MnO_6 octahedra; each block is infinite in two dimensions (xy) and n layers thick in the third (z). The A cations lie in either 12-coordinate sites within the perovskite blocks, or in nine-coordinate sites at the top and bottom of each block. The electronic properties of these materials [2] depend on the value of y and the identity of A and A' (hence the oxidation state of Mn) and also on the value of n; materials having $n=2$ show more marked CMR behavior than those having $n=1$. Detailed studies [3–5] of these manganates have shown that, in order to understand their magnetotransport behavior, it is necessary to understand a number of complex phenomena that can occur, for example charge ordering and orbital ordering. One strategy which we have followed in order to gain this understanding has involved diluting the Mn sublattice with diamagnetic cations in an attempt to produce a 1:1 ordered cation array, thus eliminating the nearest-neighbor interaction in the perovskite sheets and allowing the next-nearest-neighbor interaction to be studied in isolation. Our previous work has included [6] a study of the structural chemistry and magnetic properties of the $n=1$ Ruddlesden–Popper phases La_4LiMnO_8 and $La_3SrLiMnO_8$. We showed, by a combination of diffraction techniques (X-ray, neutron and electron), MASNMR spectrometry, magnetometry and electron microscopy that the Li and Mn cations in these materials order in a 1:1 chequer-board pattern in the sheets of vertex-sharing octahedra which lie perpendicular to the z-axis of the tetragonal unit cell. However, the sheets stack randomly along that axis, so that the cation ordering is only two dimensional (2D). The characteristics of the crystal structure are reflected in the magnetic properties and we

*Corresponding author. Fax: 44-1865-2726-90.
E-mail address: peter.battle@chem.ox.ac.uk (P.D. Battle).

0022-4596/$ - see front matter © 2003 Elsevier Inc. All rights reserved.
doi:10.1016/S0022-4596(03)00333-5

were able to show that $La_3SrLiMnO_8$, containing the cation Mn^{4+}:$^4A_{1g}$ is an excellent example of a quadratic 2D Heisenberg antiferromagnet. We described the statistical distribution of 2D ordered sheets along [001] as paracrystalline, a concept which had been developed some years earlier by Hosemann and Hindeleh [7,8]. We have since shown, albeit in a less detailed investigation [9], that other $n = 1$ RP phases, for example $La_2Sr_2BMnO_8$ (B = Mg, Zn), are also paracrystalline. These studies emphasized that the properties of these materials can only be related to the crystal structure if the latter is determined over a length scale which is shorter than that sampled in an X-ray or neutron diffraction experiment. In this paper we describe experiments intended to ascertain whether similar structural chemistry is to be found in $n = 2$ RP phases, specifically La_3LiMnO_7.

2. Experimental

A polycrystalline sample of La_3LiMnO_7 was prepared by standard solid-state techniques. Stoichiometric quantities of La_2O_3 and MnO_2 were intimately ground together with an excess of Li_2CO_3. The mixture was initially heated at 800°C for a total of 16 h, with frequent regrinding, and finally at 900°C for 2 h, with intermittent regrinding. The progress of the reaction was monitored by X-ray powder diffraction, and it was deemed to be complete when further firing produced no change in the diffraction pattern. A Siemens D5000 diffractometer operating at room temperature with Cu$K\alpha_1$ radiation was used to collect X-ray data from the final product over the angular range $10 \leqslant 2\theta(\text{deg}) \leqslant 110$, with $\Delta 2\theta = 0.02°$. The magnetic susceptibility of the product was measured over the temperature range $5 \leqslant T$ (K) $\leqslant 300$ in an applied field of 100 Oe; data were collected after cooling the sample in the measuring field (FC) and after cooling in zero field (ZFC). The magnetization was measured as a function of applied field ($-50 \leqslant H$ (kOe) $\leqslant 50$) at 5, 50 and 100 K. Time-of-flight neutron powder diffraction data were collected on the special environment powder diffractometer (SEPD) at Argonne National Laboratory. The sample (~ 5 g), contained in a thin-walled, cylindrical vanadium can, was loaded into a "Coolpower" displex refrigerator for data collection at 295 and 5 K. Data were collected over three detector banks at $2\theta = 145°$, 90° and 44°, covering the d-spacing range $0.33 < d$ (Å) < 10.21. They were analysed by the Rietveld method [10], as implemented in the GSAS package [11]. Goodness-of-fit parameters quoted below refer to the three combined datasets. MASNMR spectra were recorded on a CMX200 spectrometer at an operating frequency of 29.44 MHz for ^{6}Li, with $\pi/2$ pulse lengths of 2.5 μs and a spinning speed of 15 kHz. Electron diffraction patterns and high-resolution lattice images were collected using a JEOL 4000 EX transmission electron microscope ($C_s = 1.0$ mm; point resolution 1.6 Å) operated at 400 kV. Samples were prepared by suspension of a finely ground powder in hexane, which was then deposited onto a lacey carbon-covered copper grid. A double-tilt sample holder was used. The images were collected close to ideal Scherzer defocus conditions on aligned crystallites. Image simulations were performed using the structure refined from room-temperature neutron powder diffraction data and standard multislice algorithms available within the EMS package [12]; the [100] projection was too thick to be modelled successfully.

3. Results

3.1. Structural chemistry

(i) *X-ray and neutron diffraction*: The X-ray powder diffraction pattern of the orange/brown reaction product was initially indexed in a body-centered tetragonal space group, $I4/mmm$, with unit cell parameters typical of an $n = 2$ RP phase ($a_I = 3.82179(5)$ Å, $c_I = 20.2816(4)$ Å). The FWHM of the 0 0 10 reflection was measured to be 0.10°, a value which lies close to the instrumental resolution of the diffractometer, and thus indicates that the phase is highly crystalline. Rietveld refinement of the X-ray data in $I4/mmm$ resulted in the following agreement indices: $R_{wp} = 10.32\%$, $\chi^2 = 2.1$. The absence of superlattice peaks in the X-ray diffraction pattern is conclusive evidence that no long-range ordering of the Li^+ and Mn^{4+} cations occurs. However, the neutron diffraction pattern collected at 300 K contained Bragg peaks that could not be indexed in the simple $I4/mmm$ structure. Some of them were attributable to unreacted Li_2CO_3, and the remainder were accounted for when the pattern of the principal $n = 2$ phase was indexed in space group $P4_2/mnm$ with $a = \sqrt{2}a_I$, $c = c_I$. This space group, which is also adopted by $Sr_2YMn_2O_7$ and $Sr_2HoMn_2O_7$ [13], allows rotation of the vertex-sharing octahedra but it does not allow cation ordering over the six-coordinate sites. A two-phase (Li_2CO_3. and La_3LiMnO_7) refinement strategy, with the $n = 2$ RP compound modelled in space group $P4_2/mnm$, was therefore adopted. The unit cell parameters were determined in a reanalysis of the X-ray data in $P4_2/mnm$ and they were then held constant during analysis of the neutron diffraction data collected at room temperature; this approach allowed the refinement of the SEPD instrumental parameters. The structural parameters and bond lengths resulting from this refinement are presented in Tables 1–3. The observed and calculated diffraction profiles are shown in Fig. 1 and the structure is drawn in Fig. 2. No additional Bragg scattering indicative of long-range

Table 1
Structural parameters of La_3LiMnO_7 at room temperature and 5 K

		RT	5 K
a (Å)		5.4042(2)	5.39596(5)
c (Å)		20.2816(9)	20.2297(4)
V (Å^3)		592.33(7)	589.02(1)
La1	x	0.2516(5)	0.2508(4)
	U_{eq} (Å^2)	0.0049	
La2	x	0.2560(3)	0.2577(3)
	z	0.17850(6)	0.17853(6)
	U_{eq} (Å^2)	0.0069	
Mn/Li	x	0.259(1)	0.259(1)
	z	0.4052(2)	0.4056(2)
	U_{eq} (Å^2)	0.0119	
O1	x	0.2308(9)	0.2266(7)
	U_{eq} (Å^2)	0.0172	
O2	x	0.2309(6)	0.2267(5)
	z	0.29704(9)	0.2973(1)
	U_{eq} (Å^2)	0.0133	
O3	z	0.0965(4)	0.0969(3)
	U_{eq} (Å^2)	0.0096	
O4	z	0.1021(5)	0.1026(4)
	U_{eq} (Å^2)	0.0061	
O5	z	0.4095(4)	0.4115(3)
	U_{eq} (Å^2)	0.0135	
R_{wp} (%)		5.46	6.07
χ^2		2.532	2.139

La1 on 4f x, x, 0; La2 on 8j x, x, z; Li/Mn each 50% on 8j x, x, z; O1 4 g x, $-x$, 0; O2 on 8j x, x, z; O3 on 8h 0, 0.5, z; O4 on 4e 0, 0, z; O5 on 4e 0, 0, z.
Note: The concentration of Li_2CO_3 refined to be 10.2(8)% by weight.

Table 2
Anisotropic atomic displacement parameters (Å^2) for La_3LiMnO_7 at room temperature and 5 K

		RT	5 K
La1	U11	0.0055(6)	0.0013(5)
	U33	0.0037(8)	0.0004(7)
	U12	0.007(2)	−0.005(2)
La2	U11	0.0084(4)	0.0056(4)
	U33	0.0037(5)	−0.0001(5)
	U12	−0.008(1)	0.003(1)
	U13	−0.0006(6)	0.0001(6)
Mn/Li	U11	0.008(1)	0.008(1)
	U33	0.019(2)	0.013(2)
	U12	0.007(4)	0.011(3)
	U13	0.017(2)	0.018(2)
O1	U11	0.017(2)	0.014(2)
	U33	0.017(2)	0.012(1)
	U12	0.016(4)	0.015(3)
O2	U11	0.014(1)	0.0064(9)
	U33	0.011(1)	0.009(1)
	U12	−0.006(3)	−0.005(2)
	U13	0.0038(8)	0.0027(6)
O3	U11	−0.003(2)	0.004(2)
	U22	0.022(3)	0.024(3)
	U33	0.011(2)	0.004(2)
	U12	−0.010(1)	−0.007(2)
O4	U11	0.001(2)	−0.007(1)
	U33	0.017(3)	0.012(2)
	U12	0.001(2)	−0.001(2)
O5	U11	0.021(3)	0.008(2)
	U33	−0.001(2)	0.000(2)
	U12	0.016(2)	0.008(2)

magnetic ordering was apparent in the neutron diffraction data collected at 5 K, and a satisfactory structural refinement was again accomplished in space group $P4_2/mnm$. The refined parameters are included in Tables 1 and 2. The unit cell parameters were allowed to vary in this analysis, with the instrumental parameters held fixed at the values determined in the analysis of the data collected at room temperature. At 5 K, the atomic displacement parameters associated with the La^{3+} cations take values which are plausible for a well-ordered structure whereas some components of those associated with the Li/MnO_6 sublattice are larger than might be expected.

(ii) *^{6}Li MASNMR*: The NMR spectrum of La_3LiMnO_7 shown in Fig. 3 consists of a single resonance with a large negative hyperfine shift ($\delta = -479$ ppm). The width of the resonance is comparable to that observed from La_4LiMnO_8, and it is certainly narrower than that from $La_3SrLiMnO_8$. As was described above, we have previously shown that both of these compounds contain a 2D 1:1 ordered array of Li and Mn cations in an $n = 1$ RP structure, and that the presence of only a single, sharp NMR resonance is symptomatic of this ordering. Similarly, the narrow linewidth illustrated in Fig. 3 leads us to conclude that there is only one local Li environment in La_3LiMnO_7, and that the six-coordinate cations in this compound order in a regular manner within each of the perovskite-like double layers apparent in Fig. 1(a). This conclusion does not lie easily with the analysis of the neutron diffraction data in space group $P4_2/mnm$ which constrains all the octahedral sites to be equivalent.

Table 3
Bond lengths (Å) and bond angles (deg) in La_3LiMnO_7 at room temperature

La1–O1 × 2	2.610(5)	O1–Li/Mn–O2	176.8(6)
La1–O1 × 2	2.799(5)	O1–Li/Mn–O3	91.1(3)
La1–O3 × 4	2.735(6)	O1–Li/Mn–O4	92.2(5)
La1–O4 × 2	2.826(8)	O1–Li/Mn–O5	89.9(4)
La1–O5 × 2	2.641(6)	O2–Li/Mn–O3	88.8(3)
La2–O2 × 1	2.412(2)	O2–Li/Mn–O4	91.0(4)
La2–O2 × 2	2.882(4)	O2–Li/Mn–O5	87.0(4)
La2–O2 × 2	2.615(4)	O3–Li/Mn–O3	175.5(6)
La2–O3 × 2	2.534(5)	O3–Li/Mn–O4	91.9(3)
La2–O4 × 1	2.496(6)	O3–Li/Mn–O5	88.1(3)
La2–O5 × 1	2.581(6)	O4–Li/Mn–O5	178.0(5)
Li/Mn–O1 × 1	1.925(4)	Li/Mn–O1–Li/Mn	175.2(7)
Li/Mn–O2 × 1	2.203(5)	Li/Mn–O3–Li/Mn	178.0(6)
Li/Mn–O3 × 2	1.9121(4)	Li/Mn–O4–Li/Mn	170.9(6)
Li/Mn–O4 × 1	1.850(9)	Li/Mn–O5–Li/Mn	175.0(5)
Li/Mn–O5 × 1	1.979(9)		

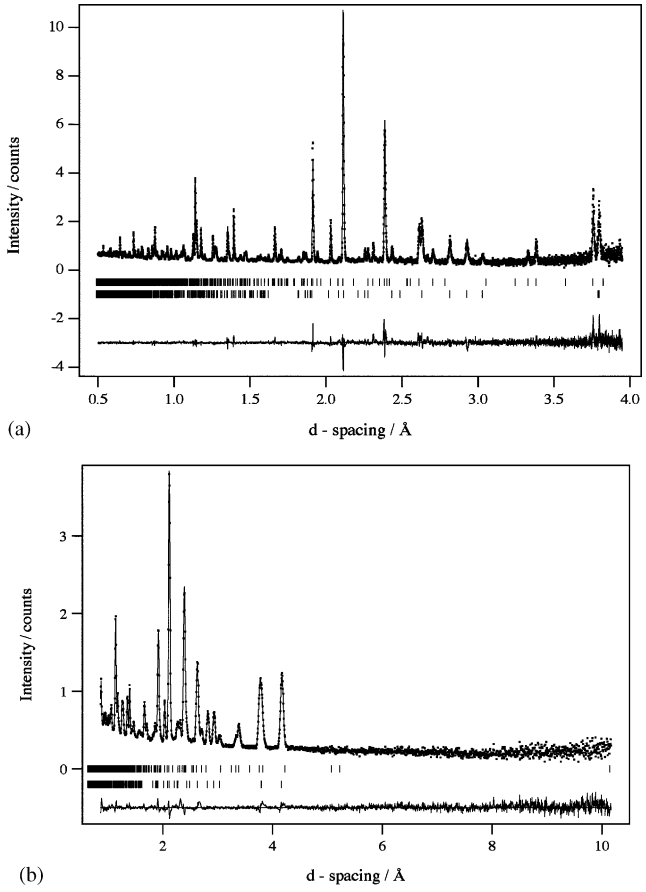

Fig. 1. Observed (.), calculated (-) and difference neutron powder diffraction profiles of La_3LiMnO_7 recorded at room temperature (a) $2\theta = 145°$, (b) $2\theta = 44°$. Reflection positions are marked; upper tick marks La_3LiMnO_7, lower tick marks Li_2CO_3.

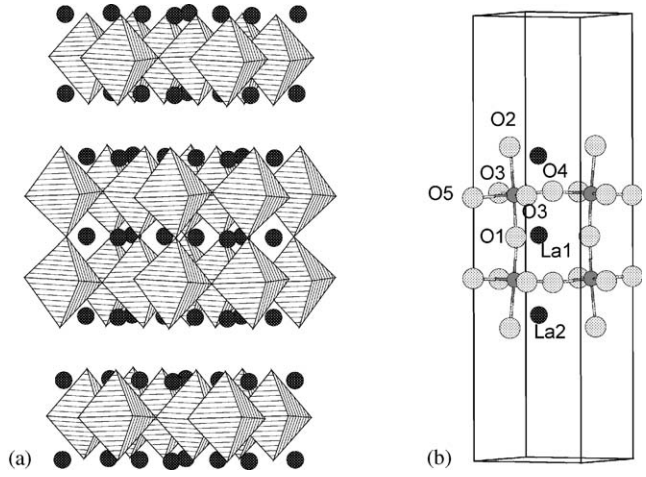

Fig. 2. Representations of the crystal structure of La_3LiMnO_7 as determined by neutron diffraction: (a) Li/MnO_6 octahedra and La atoms; (b) local atomic arrangement in a bilayer.

The hyperfine shifts in these and related compounds depend strongly on the number and arrangements of the paramagnetic ions in the lithium local environment

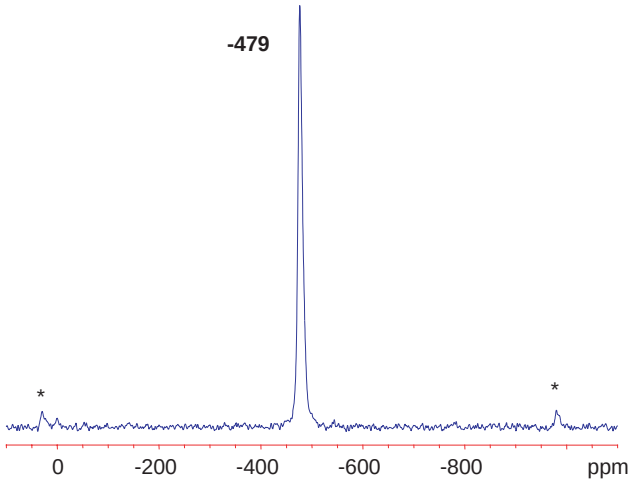

Fig. 3. The ^6Li MAS NMR spectrum of La_3LiMnO_7. The isotropic resonance is marked with its corresponding hyperfine shift. The very weak resonance at around 0 ppm is due to diamagnetic impurities such as lithium carbonate. Spinning sidebands are also marked (*).

[14,15]. In La_4LiMnO_8, each Li is coordinated to four Mn^{4+} ions via Li–O–Mn^{4+} connectivities with 180° bond angles. Each "180°-interaction" contributes approximately −125 ppm, at room temperature, to the hyperfine shift, resulting in an overall shift for La_4LiMnO_8 of –500 ppm [6]. Assuming strict alternation of Li^+ and Mn^{4+} in La_3LiMnO_7, each Li is connected to five Mn^{4+} ions, and a shift of approximately –626 ppm is predicted, assuming 180° Li–O–Mn bond angles. This calculated shift is much larger than that observed experimentally.

Previous NMR studies have shown that the hyperfine shift depends strongly on the Li–O–Mn bond angle, increasing from –125 to more than 250 ppm as the Li–O–Mn bond angle is decreased from 180° to 90°. At 180°, the major source of the hyperfine shift involves an interaction with the e_g orbitals on the Mn^{4+} ions, while at 90°, the shift is dominated by an interaction involving the 1/2-filled t_{2g} orbitals. Intermediate angles, as found for example in a series of spinels, result in intermediate values for the shift. For example, in the ordered Mn(IV) spinel $(LiZn)_{0.5}(LiMn_3)_{0.5}O_4$, a bond angle of 120.6° results in a shift of +76 ppm, per Li–O–Mn interaction [16]. The smaller shift observed for La_3LiMnO_7 appears to indicate that the Li–O–Mn linkages are non-linear in this compound and thus provides strong evidence for a tilting of the octahedra. An accurate estimate of the average Li–O–Mn bond angle is difficult given the limited number of model compounds that have been studied to date. However, on the basis of an average shift per Li–O–Mn interaction of –95 ppm in La_3LiMnO_7, a mean Li–O–Mn bond angle of between 160° and 170° would appear reasonable. This is somewhat smaller than the values (Table 3) calculated from the disordered average structure determined by neutron

diffraction. Although additional factors such as the difference between the Mn–O and Li–O bond lengths of different compounds are also important in controlling the size of the hyperfine shifts, it is not necessarily clear that this is the source of the discrepancy. A very small decrease in the average Li/Mn–O bond length is observed on moving from La_4LiMnO_8 to La_3LiMnO_7, which should result in a slightly larger hyperfine shift for La_3LiMnO_7 (and thus an even smaller value for the predicted Li–O–Mn bond angle). The NMR experiments probe local distortions; these may not be observed by the neutron diffraction experiments, which cannot distinguish between Li and Mn (because of their similar scattering lengths) and provide only average Li, Mn and O positions. This averaging is the cause of the high atomic displacement parameters referred to above and listed in Table 2. Thus, it may be that the Li–O–Mn bond angles are smaller than implied by the neutron diffraction results.

(iii) *Electron diffraction and microscopy*: Electron diffraction patterns taken along various zone axes of La_3LiMnO_7 are shown in Figs. 4(a)–(c) and lattice images in Figs. 4(d) and (e). Superlattice reflections attributable to the tilting of the octahedra are visible in Fig. 4(a). The [100] zone shown in Fig. 4(c) is of particular interest; the diffraction pattern shown is typical of those observed, although there was some variation between different crystallites. The discrete reflections visible in the pattern can all be indexed in space group $P4_2/mnm$, but lines of diffuse scattering, which can be indexed as $0k\xi$, $k = 2n + 1$, are also apparent. The presence of these lines demonstrates that although the crystal structure is well defined in 2D (the xy plane), the periodic character is less well established along the z-axis. The diffraction pattern thus provides evidence that this $n = 2$ RP phase might show paracrystallinity similar to that observed previously in $n = 1$ phases. However, intensity maxima corresponding to Bragg peaks are apparent on the lines, for example at 0 1 2, and the structure is therefore not completely disordered along [001]. Furthermore, the intensity maxima on these lines do not correspond to reflections allowed in $P4_2/mnm$, suggesting that the local structure has a different symmetry. This fine structure was not observed on the lines of diffuse scattering generated by the $n = 1$ phases, and we take this as evidence that the average size of a coherent structural region is greater in the case of the $n = 2$ material. Support for this hypothesis is provided by the lattice image shown in Fig. 4(e), which is best considered along with the idealized structural projections shown in Fig. 5. Ordering of the Li and Mn cations would lead to a reduction in the symmetry of the structure, and one possible ordering scheme, which can be accommodated in the monoclinic space group $P2_1$, is illustrated in Fig. 5. The

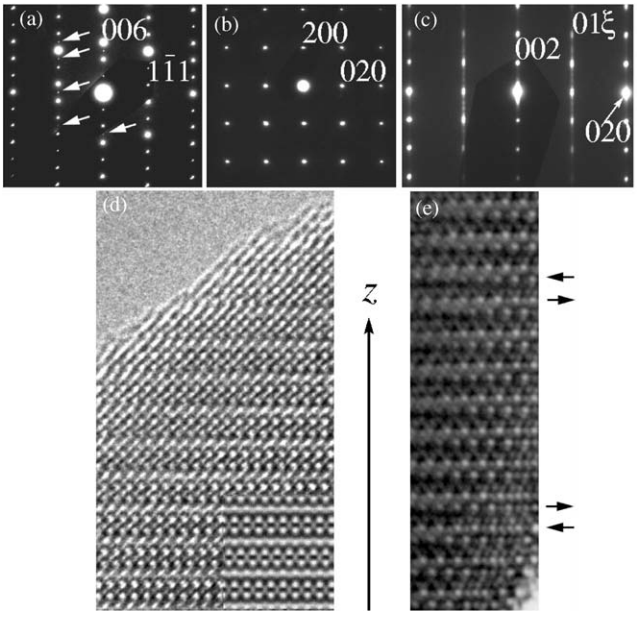

Fig. 4. (a) [110], (b) [001], and (c) [100] SAED patterns of La_3LiMnO_7 with superlattice reflections are arrowed in (a); (d) [110] HRTEM image, with calculated image (−8 nm defocus, 8 unit cells thick) shown in inset; (e) [100] HRTEM image, with stacking faults indicated by horizontal arrows.

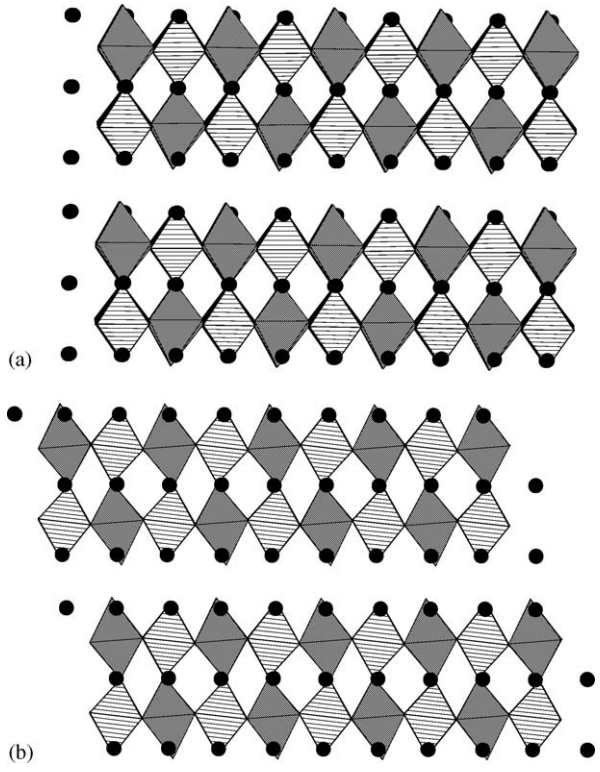

Fig. 5. Projection of the structure of cation-ordered La_3LiMnO_7 along (a) [010] and (b) [100] of the tetragonal unit cell. Shaded and hatched octahedra represent LiO_6 and MnO_6 groups. The zig-zag chains of each type of octahedron are in phase in adjacent bilayers in (a) and out of phase in (b).

in-plane unit cell parameters of this structure are not constrained by symmetry to be identical, but we assume them to be equal. The two parts of the figure show perpendicular views of the hypothetical ordered structure along directions close to [100] and [010] of the tetragonal unit cell; the degree of octahedral tilting shown in the figure is illustrative and arbitrary. Each chain of octahedra parallel to the viewing direction contains only one cation type, either Li or Mn. However perpendicular to the viewing direction, zig-zag chains of both MnO_6 and LiO_6 octahedra can be seen within each bilayer. In Fig. 5(a) these chains are in phase with those in the neighboring bilayer, whereas in Fig. 5(b) the chains in neighboring bilayers are out of phase. The occurrence of anti-site ordering, equivalent to a displacement of one layer with respect to its neighbor, will therefore have the effect of rotating the apparent viewing direction by 90°. Consideration of Fig. 4(e) allows the recognition of zig-zag chains of contrast in the scattering density within the bilayers (best seen by looking at the pattern of strong white spots). The relative phase of the zig-zags in adjacent bilayers changes twice in Fig. 4(e); the layers involved are marked by arrows. Thus, within the distance $\sim 6c_I$ (~ 120 Å) shown in the image, the relative phase of adjacent bilayers changes twice, with each boundary appearing as a switch in the viewing direction between [100] and [010]. The structural domains on either side of the boundary are displaced with respect to each other in projection by the width of one octahedron. We therefore believe that the Mn and Li cations in this compound adopt a 1:1 ordered arrangement within each bilayer, but that the alignment of neighboring cation-ordered bilayers along [001] is not regular over distances greater than ~ 60 Å. The cation ordering is not apparent in the [110] lattice image (Fig. 4(d)), which is well simulated by a disordered model, because the Li and Mn cations alternate in the chains of octahedra parallel to this axis. The local space-group symmetry of the structure must be lower than $P4_2/mnm$ and we have devised a feasible model in the monoclinic space group $P2_1$, but we do not claim to have proved this to be the correct symmetry. The symmetry lowering is consistent with the occurrence of non-linear Li–O–Mn bond angles, as suggested by the low value of the NMR shift.

3.2. Magnetic properties

The molar magnetic susceptibility of La_3LiMnO_7 is shown in Fig. 6. The FC and ZFC data overlie throughout the measured temperature range, and the susceptibility passes through a maximum at 14 K. The data collected above 115 K can be fitted to a Curie–Weiss law with $\mu_{eff} = 3.74\,\mu_B$ and $\theta = -73$ K; the value of the effective magnetic moment agrees well with the spin-only value ($3.87\,\mu_B$) for Mn^{4+}. The field dependence of the

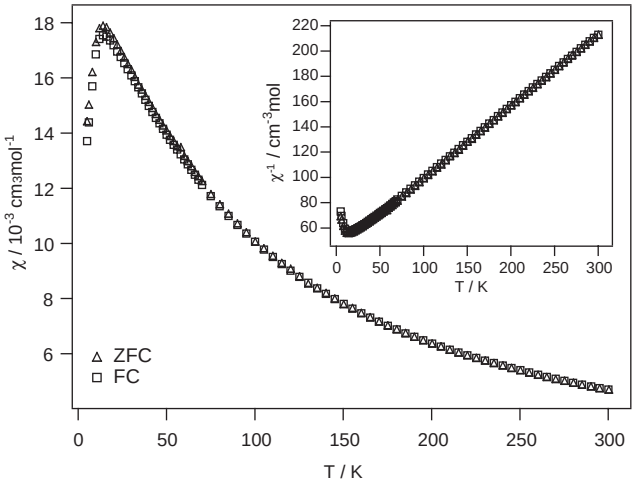

Fig. 6. Temperature dependence of the molar FC and ZFC magnetic susceptibility of La_3LiMnO_7.

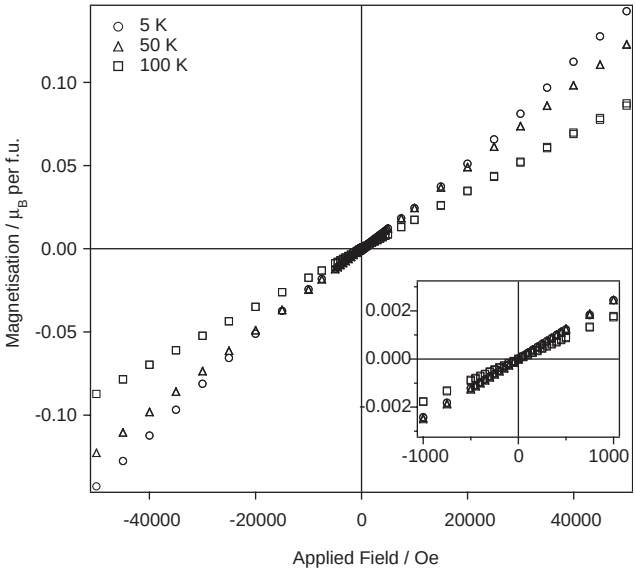

Fig. 7. Field dependence of the magnetization (per formula unit) of La_3LiMnO_7 as a function of temperature.

magnetization per formula unit is illustrated in Fig. 7. The increased gradient of the data measured at 5 K in fields >20 kOe can be attributed to the onset of a spin-flop transition. No hysteresis is apparent, and the data presented in Figs. 6 and 7 together suggest that, in low fields, La_3LiMnO_7 orders antiferromagnetically at 14 K. However, this is inconsistent with the absence from the low-temperature neutron diffraction pattern of magnetic Bragg scattering. We shall return to this point below.

4. Discussion

In order to rationalize the electron diffraction and microscopy data with the X-ray, neutron and NMR

studies described above, we have proposed that the Mn and Li cations are ordered in a 1:1 manner within each bilayer. However, the ordering is only coherent for relatively short distances along the direction perpendicular to the bilayers. The coherent regions of cation ordering are too small to influence the results of the neutron and X-ray diffraction experiments, and the average structure seen by these probes is cation-disordered and tetragonal. However, NMR is a local probe, and thus detects just one Li environment in the cation-ordered bilayers. The coherence length of the electron beam in the microscope is shorter than those of the X-ray and neutron beams and the disorder in the bilayer stacking sequence is revealed by lines of diffuse scattering in the electron diffraction pattern. However, whereas the stacking of successive layers in the $n = 1$ materials La_4LiMnO_8 and $La_3SrLiMnO_8$ was shown to be random, the electron diffraction patterns show that ordered regions of finite size do exist in the $n = 2$ material, and this material therefore cannot be described as being paracrystalline with a 50% (i.e. random) stacking probability. It is better described either as paracrystalline with a biased stacking probability or as a cation-ordered, monoclinic material with a sufficiently high concentration of stacking faults, in the form of anti-site ordering domains, to cause it to appear disordered and tetragonal to any probe with a sampling distance greater than ~ 60 Å. This difference in behavior may be attributable to the tilting of the octahedra which is present in the $n = 2$ system but not in the $n = 1$ compounds described previously, and which will remove the degeneracy of the possible orientations of successive bilayers.

The apparent incompatibility between the magnetometry data, which all point to an antiferromagnetic ground state in weak (<20 kOe) fields, and the low-temperature neutron diffraction data can also be explained within this model if we assume that antiferromagnetic order occurs within each structural block, the size of the block being limited along z by the occurrence of anti-site ordering at intervals of ~ 60 Å, but that there is no magnetic coherence between adjacent blocks. Simplistically, regions separated by two stacking faults, that is regions which might be expected to have the same layer orientation, would have only a 50% probability of having the same spin structure; they are equally likely to suffer spin reversal and form antiparallel domains. In fact, the monoclinic symmetry proposed for the local structure would mean that each type of bilayer has two slightly different orientations (this follows from the two possible directions of the unique axis, $\beta = 90 \pm \delta$) and regions separated by two stacking faults are not necessarily exactly aligned with each other. Thus the incoherent nature of the long-range crystal structure destroys the long-range coherence of the magnetic structure in a way that eliminates magnetic Bragg scattering.

In conclusion, it is clear that the crystal chemistry of $n = 2$ La_3LiMnO_7 has many parallels with that of the $n = 1$ compounds La_4LiMnO_8 and $La_3SrLiMnO_8$ but that significant differences are introduced by the increased thickness of the perovskite bilayers. The underlying point, that neutron and X-ray diffraction data on these phases must be interpreted with caution, remains.

Acknowledgments

We thank EPSRC, the Royal Society (a Research Fellowship for JS) and NSF (Grant DMR0211353 to CPG) for financial support. The submitted manuscript has been created by the University of Chicago as Operator of Argonne National Laboratory ('Argonne') under Contract W-31-109-ENG-38 with the U.S. Department of Energy. The U.S. Government retains for itself, and others acting on its behalf, a paid-up, nonexclusive, irrevocable worldwide license in said article to reproduce, prepare derivative works, distribute copies to the public, and perform publicly and display publicly, by or on behalf of the Government.

References

[1] S.N. Ruddlesden, P. Popper, Acta Crystallogr. 11 (1958) 541.
[2] P.D. Battle, M.J. Rosseinsky, Curr. Opin. Solid State Mater. Sci. 4 (1999) 163.
[3] D.N. Argyriou, H.N. Bordallo, B.J. Campbell, A.K. Cheetham, D.E. Cox, J.S. Gardner, K. Hanif, A.d. Santos, G.F. Strouse, Phys. Rev. B 61 (2000) 15269.
[4] T. Kimura, R. Kumai, Y. Tokura, J.Q. Li, Y. Matsui, Phys. Rev. B 58 (1998) 11081.
[5] C.D. Ling, J.E. Millburn, J.F. Mitchell, D.N. Argyriou, J. Linton, H.N. Bordallo, Phys. Rev. B 62 (2000) 15096.
[6] J.C. Burley, P.D. Battle, D.J. Gallon, J. Sloan, C.P. Grey, M.J. Rosseinsky, J. Amer. Chem. Soc. 124 (2002) 620.
[7] R. Hosemann, Zeit. Phys. 128 (1950) 465.
[8] A.M. Hindeleh, R. Hoseman, J. Phys. C: Solid State Physics 21 (1988) 4155.
[9] J.C. Burley, P.D. Battle, P.J. Gaskell, M.J. Rosseinsky, J. Solid State Chem. 168 (2002) 202.
[10] H.M. Rietveld, J. Appl. Crystallogr. 2 (1969) 65.
[11] A.C. Larson, R.B. von-Dreele, General Structure Analysis System (GSAS), Los Alamos National Laboratories, Report LAUR 86-748, 1990.
[12] P.A. Stadelman, Ultramicroscopy 21 (1987) 131.
[13] P.D. Battle, J.E. Millburn, M.J. Rosseinsky, L.E. Spring, J.F. Vente, P.G. Radaelli, Chem. Mater. 9 (1997) 3136.
[14] C. Pan, Y.J. Lee, B. Ammundsen, C.P. Grey, Chem. Mater. 14 (2002) 2289.
[15] Y.J. Lee, F. Wang, C.P. Grey, J. Amer. Chem. Soc. 120 (1999) 12601.
[16] Y.J. Lee, S.-H. Park, C. Eng, J.B. Parise, C.P. Grey, Chem. Mater. 14 (2002) 194.